JACS
JOURNAL OF THE AMERICAN CHEMICAL SOCIETY
pubs.acs.org/JACS
Communication

Epitaxial Core/Shell Nanocrystals of (Europium-Doped) Zirconia and Hafnia

Carlotta Seno, Nico Reichholf, Francesco Salutari, Maria Chiara Spadaro, Yurii P. Ivanov, Giorgio Divitini, Alexander Gogos, Inge K. Herrmann, Jordi Arbiol, Philippe F. Smet, and Jonathan De Roo*

Cite This: J. Am. Chem. Soc. 2024, 146, 20550−20555

ABSTRACT: A careful design of the nanocrystal architecture can strongly enhance the nanocrystal function. So far, this strategy has faced a synthetic bottleneck in the case of refractory oxides. Here we demonstrate the epitaxial growth of hafnia shells onto zirconia cores and pure zirconia shells onto europium-doped zirconia cores. The core/shell structures are fully crystalline. Upon shelling, the optical properties of the europium dopant are dramatically improved (featuring a more uniform coordination and a longer photoluminescence lifetime), indicating the suppression of nonradiative pathways. These results launch the stable zirconium and hafnium oxide hosts as alternatives for the established $NaYF_4$ systems.

Zirconium and hafnium oxide nanocrystals (NCs) are appealing (host) materials due to their high thermal and chemical stability and large band gap.[1] Colloidal ZrO_2 NCs are components for (in)organic composites,[2−4] while HfO_2 NCs find applications in memory devices.[5,6] Due to the high atomic number of hafnium and the high density of hafnia, HfO_2 NCs have been developed as computed tomography contrast agents,[7−9] scintillators,[10] and radiation therapy enhancers.[11−13]

Both ZrO_2 and HfO_2 NCs serve as hosts for optically active lanthanide ions, e.g., europium.[1,14−18] Fluorides (e.g., $NaYF_4$ and $NaGdF_4$) are another class of nanocrystals that are widely used as hosts for lanthanides, with application in upconversion and downconversion.[19−23] In the fluoride system, the syntheses are well-developed, allowing for the precise positioning of dopants inside the nanocrystal and the growth of undoped shells on the doped core. The latter results in core/shell architectures, which were pioneered in the field of semiconductor nanocrystals (quantum dots) to prevent the excited electrons and holes from interacting with surface traps.[24,25] Likewise, shelling protects the lanthanides from surface effects and thus increases the quantum efficiency of both up- and downconversion processes.[26] Additionally, multilayered structures offer controlled energy cascades in the case of lanthanide-doped fluorides.[27] Higher quantum efficiencies coupled with long lifetimes enabled their use in, e.g., time-gated fluorescence imaging.[15,28] The oxide hosts have found less widespread use because of the synthetic challenge of producing colloidally stable oxide nanocrystals with a complex (e.g., core/shell) architecture.[29] However, the oxide hosts are more chemically stable, while the fluorides dissolve in highly dilute aqueous media.[30]

Surfactant-assisted, nonaqueous synthesis methods have allowed the synthesis of ZrO_2 and HfO_2 NCs with control over their size.[1,31−37] Even more, solid solutions of various compositions ($Zr_xHf_{1-x}O_2$) were obtained as colloidal nanocrystals.[34,38,39] $Hf_{0.5}Zr_{0.5}O_2$ is an interesting ferroelectric material, making it promising for nonvolatile memory devices.[40,41]

Here we leverage the control of nonaqueous synthesis and report metal oxide core/shell nanocrystals. We epitaxially grow HfO_2 (or ZrO_2) onto ZrO_2 and ZrO_2 onto ZrO_2:Eu^{3+}. The beneficial effect of the shell on the optical properties of the europium dopant is established. Having access to these novel heterostructures, which are unavailable in bulk, opens up possibilities for their application in different areas, from microelectronics to scintillators.

Zr and Hf are chemically very similar, and both oxide nanocrystals can be synthesized at 340 °C from the metal chloride and isopropoxide in tri-*n*-octylphosphine oxide (TOPO).[1] Under these conditions, HfO_2 forms nanorods with the monoclinic crystal structure, while ZrO_2 forms spherical nanocrystals with the tetragonal crystal structure. We first focus on the ZrO_2/HfO_2 core/shell structure, since one can conveniently distinguish growth of HfO_2 onto the spherical ZrO_2 cores from separately nucleating HfO_2 nanorods. ZrO_2 and HfO_2 form similar crystal structures (monoclinic, tetragonal, and cubic) with negligible lattice mismatch, thus allowing for epitaxial growth. We followed a two-step approach toward the core/shell structure. In the first step, we synthesized and isolated ZrO_2 cores from $ZrCl_4$ and $Zr(O^iPr)_4{\cdot}^iPrOH$ in TOPO (Figure 1A).[42] The cores are spherical with an average diameter of 3.8 nm according to bright-field transmission electron microscopy (BF TEM)

Received: April 12, 2024
Revised: May 27, 2024
Accepted: July 5, 2024
Published: July 22, 2024

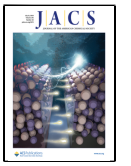

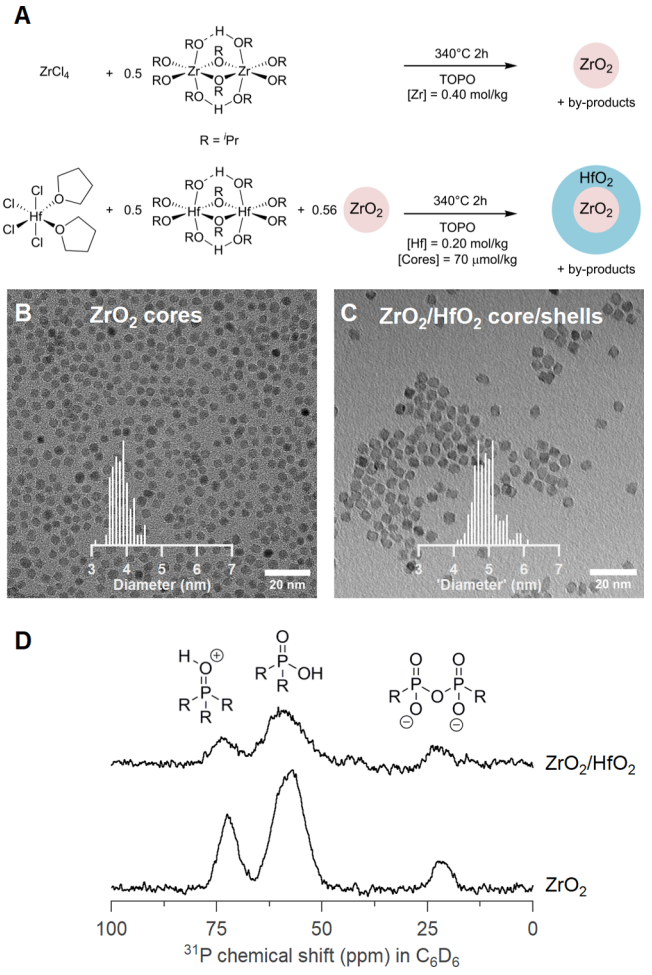

Figure 1. (A) ZrO_2 core and ZrO_2/HfO_2 core/shell synthesis procedure, where the metal chloride, tetrahydrofuran, propene, and isopropanol are obtained as byproducts.[31,32] (B, C) BF TEM images of (B) ZrO_2 cores and (C) ZrO_2/HfO_2 core/shells. The histograms are based on more than 100 particles. (D) Solution ^{31}P NMR spectra of ZrO_2 and ZrO_2/HfO_2 NCs.

(Figure 1B). The cores have the tetragonal ($P4_2/nmc$) crystal structure (Figures S1 and S2), and their surface is covered with a mixture of protonated TOPO, dioctyl phosphinate, and dioctyl pyrophosphonate (Figure 1D).[42] In a second step, the purified cores were added to a new reaction mixture of $HfCl_4(THF)_2$ and $Hf(O^iPr)_4{\cdot}^i$PrOH in TOPO (see Figure 1A). After 2 h at 340 °C, the core/shell structures were isolated and purified. The nanocrystal surface is covered by the same ligands as mentioned before (see Figure 1D for the ^{31}P NMR spectrum). Atomic-resolution high-angle annular dark-field (HAADF) scanning TEM (STEM) analysis shows that the resulting nanocrystals are no longer spherical but more clearly faceted, exposing $\{01\bar{1}\}$ and $\{10\bar{1}\}$ surfaces (Figures S3 and S4). To be able to compare the sizes of core and core/shell particles, we analyze the BF TEM image (Figure 1C) by measuring the projected area of the faceted nanocrystals and calculating an apparent "diameter", which is the diameter for a circle with equal area. The core/shell structures have an average "diameter" of 4.9 nm, clearly indicating that the cores (d = 3.8 nm) have grown to larger sizes. Crystal growth is further confirmed by the narrower reflections in X-ray diffraction (XRD) (Figure S1) and extended features in the pair distribution function (PDF) (Figure S2).

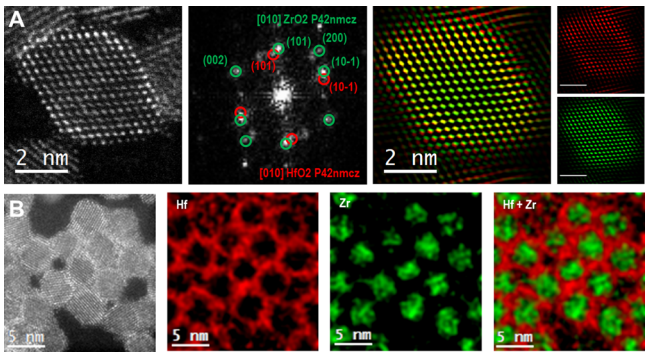

Figure 2. (A) HAADF STEM image of a core/shell ZrO_2/HfO_2 nanocrystal, the corresponding power spectrum (FFT) analysis in the reciprocal space along the [010] zone axis, and the frequency-filtered map HAADF STEM image. (B) HAADF STEM image of several ZrO_2/HfO_2 nanocrystals and the corresponding EDX compositional maps featuring hafnium and zirconium.

The core/shell interface was further analyzed by atomic-resolution HAADF STEM (see Figures 2, S3, and S4). From the contrast in Figure 2A, we can recognize the presence of a core/shell structure, as the shell appears brighter with respect to the core due to the higher atomic number of Hf compared to Zr. The power spectrum (FFT) analysis in the reciprocal space shows that the ZrO_2 core has the $P4_2/nmc$ tetragonal structure and that the HfO_2 shell has a similar structure. Tetragonal HfO_2 has the following lattice parameters at room temperature: $a = b = 3.65$ Å, $c = 5.33$ Å. These are slightly higher than those of tetragonal ZrO_2: $a = b = 3.59$ Å, $c = 5.18$ Å.[43,44] This is in good agreement with the observed crystal arrangement in our core/shell nanoparticles. The (101) and $(10\bar{1})$ reflections are "elongated" or doubled, indicating the presence of HfO_2 that grows epitaxially and partially relaxed onto the indicated surfaces of the ZrO_2 core. The frequency-filtered map clearly displays the core in green and the shell in red.

While pure HfO_2 nanocrystals would crystallize in the monoclinic $P2_1/c$ structure, epitaxial growth thus stabilizes hafnia in its tetragonal structure. Final confirmation of the core/shell structure is provided by energy-dispersive X-ray spectroscopy (EDX) compositional mapping, which shows regions with zirconium in the center and hafnium in the shell (Figure 2B). When shelling the zirconia cores with zirconia shells under identical conditions, we cannot infer the success from compositional mapping. However, the final core/shell particles had an average "diameter" of 5.5 nm, indicating successful growth (Figure S5).

Second, we turn to the optically active ZrO_2:Eu/ZrO_2 core/shell system. We synthesized europium-doped zirconia (10.0% nominal doping) from europium acetate, zirconium propoxide, and benzyl alcohol (Figure 3A).[15] After synthesis, we functionalized the nanocrystal surface with dodecanoic acid ligands (Figure S6). The ZrO_2:Eu cores have an average diameter of 3.5 nm (Figure 3B), possess the tetragonal crystal structure (Figures S1 and S2), and have an actual doping concentration of 9.0% (determined by ICP-OES). The efficient incorporation of europium into the oxide lattice is in agreement with previous reports.[15−17]

The cores were subjected to a shelling procedure using $ZrCl_4(THF)_2$ and $Zr(O^iPr)_4{\cdot}^i$PrOH (Figure 3A). After 2 h at 340 °C, colloidally stable nanocrystals were isolated and purified (Figure S7 for ^{31}P NMR and Figure S8 for DLS). BF

https://doi.org/10.1021/jacs.4c05037
J. Am. Chem. Soc. 2024, 146, 20550−20555

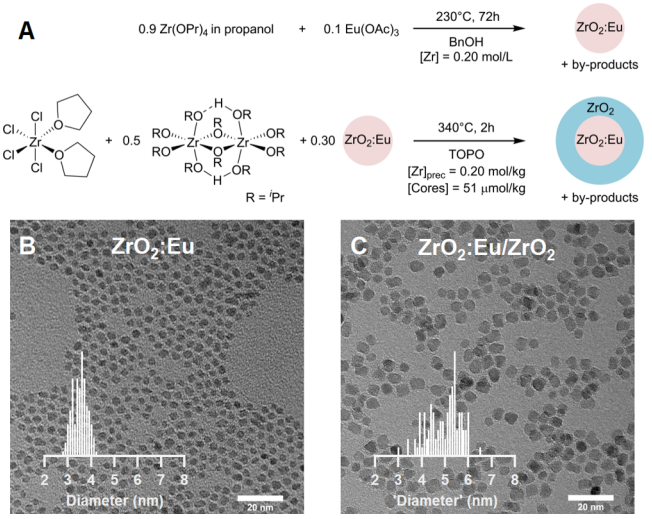

Figure 3. (A) ZrO_2:Eu core and ZrO_2:Eu/ZrO_2 core/shell syntheses. (B, C) BF TEM images of (B) ZrO_2:Eu cores and (C) ZrO_2:Eu/ZrO_2 core/shells. The histograms are based on more than 100 particles.

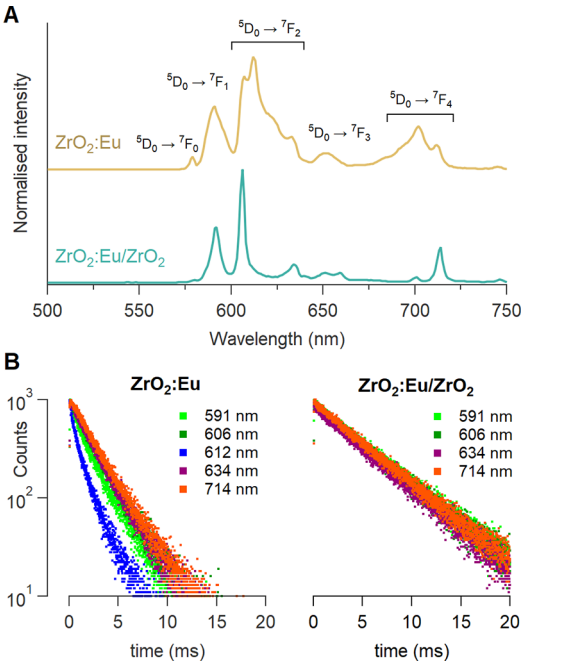

Figure 4. (A) Photoluminescence emission spectra and (B) lifetime decays at various emission wavelengths of ZrO_2:Eu cores and ZrO_2:Eu/ZrO_2 core/shells, excited at 238 nm. The measurements were carried out at room temperature in cyclohexane with an absorbance of 0.1 at 238 nm.

TEM imaging shows an increase in the average "diameter" to 5.1 nm (Figure 3C), and again, sharper reflections in XRD and extended signals in the PDFs are observed, confirming growth of the tetragonal crystal (Figures S1 and S2). HAADF STEM and powder spectrum analysis further confirm that both ZrO_2:Eu cores and ZrO_2:Eu/ZrO_2 core/shells have the tetragonal structure (Figures S9 and S10). The europium content decreases in the core/shells to 1.8% metal content. This is close to the expected 2.1% considering the stoichiometry of the reaction.

The optical properties of the europium dopant change substantially when the cores are shelled (see Figures 4A, S11, and S12). The excitation and emission spectra of Eu in the ZrO_2:Eu cores is consistent with previous reports of Eu doped into colloidal ZrO_2 nanocrystals or ZrO_2 powders.[15,17,45,46] Upon shelling, certain emission channels disappear (e.g., the emission band at 612 nm, belonging to a $^5D_0 \rightarrow {}^7F_2$ transition), and the remaining emission peaks are more narrow (Figure 4A). This indicates a change in the coordination around the europium ion. This is further demonstrated by the shape of the $^5D_0 \rightarrow {}^7F_0$ transition around 580 nm, measured at 10 K (Figure S13). This $J = 0 \rightarrow J' = 0$ transition is not split by the crystal field, and thus, spectrally different contributions for this transition can be assigned to different coordinating environments. For the core/shell, the emission band corresponding to this transition is narrower and more symmetric, indicating a highly uniform environment for europium.

The shell also has a significant impact on the lifetime of the excited state (Figure 4B). For the ZrO_2:Eu cores, the luminescence decay depends on the monitored emission wavelength but in all cases is biexponential. This variation in lifetime points again to different europium coordination environments. We fit the decay profiles using the function

$$I(t) = I_0 + a_1 e^{-t/\tau_1} + a_2 e^{-t/\tau_2} \quad (1)$$

At 606 nm, we determine a slow component of $\tau_1 = 2.7 \pm 0.1$ ms and a fast component of $\tau_2 = 1.2 \pm 0.1$ ms. The slow component contributes 86% to the total emission, calculated via

$$\phi_1 = \frac{a_1\tau_1}{a_1\tau_1 + a_2\tau_2} \quad (2)$$

For the core/shells, the decay is monoexponential and independent of the monitored wavelength (Figure 4B). We determined a lifetime of 5.3 ± 0.1 ms. This is similar to the longest values reported for Eu^{3+} in ZrO_2 (nano)powders,[47] indicating that the contribution of nonradiative decay, e.g. via interaction with surface or other defects, is limited. In the literature, long lifetimes of 4−5 ms appear only for low doping percentages (1%). Higher doping percentages are typically associated with shorter lifetimes.[47] Here we report a core doped with 9% Eu that features a lifetime of 5.3 ms after shelling and thus passivation of the surface defects. Some authors attribute the faster decay to a monoclinic crystal phase and the slower decay to the tetragonal phase.[48] Given that we find no evidence of a monoclinic phase, we assign the fast decay (present only in the ZrO_2:Eu cores) to Eu ions that are near the nanocrystal surface. Based on the changes in the emission spectrum and the increase in lifetime, we conclude that the shelling improves the incorporation of the Eu ions in the oxide crystal. Indeed, Eu^{3+} ions act as a probe for their local environment.[49−52]

While excitation of the ZrO_2:Eu/ZrO_2 core/shells at 240−260 nm yields only the 4f−4f transitions of Eu^{3+}, excitation at 300 nm generates an additional broadband contribution ranging from 350 to 600 nm related to defect emission in ZrO_2 (Figure S14).[31,53−55] The coexistence of broadband and europium emission in ZrO_2 (with 0.4% Eu doping) was recently exploited for ratiometric fluorescence thermometry in the range from 130 to 230 K.[56] We did not observe this strong broadband emission for the ZrO_2:Eu cores with high Eu doping (9%) (see Figure S14), implying that the presence of Eu ions suppresses the defect emission. This suggests that for

https://doi.org/10.1021/jacs.4c05037
J. Am. Chem. Soc. 2024, 146, 20550−20555

the core/shell particles, the Eu ions remain located in the core during the shelling, since the presence of Eu ions in the shell would suppress the ZrO_2 defect emission (either by preventing the defect from forming or by short-range energy transfer to Eu).[57−59] Therefore, the overall emission spectrum of the core/shells contains emission from Eu^{3+} in the core and defect emission from the shells. This also explains the drastic increase in the Eu^{3+} lifetime of the core/shell particles, since the Eu^{3+} ions are now in a perfect environment, shielded from the surface.

In summary, we have reported the use of crystalline zirconium or hafnium oxide to shell nanocrystals. This method was applied to improve the local environment of europium dopants in zirconia nanocrystals and to suppress nonradiative de-excitation pathways. Our results are an invitation to explore intricate nanocrystal architectures with oxide host materials.

■ ASSOCIATED CONTENT

Data Availability Statement

The data that support the findings of this study are openly available in Zenodo at DOI: 10.5281/zenodo.12684072.

Supporting Information

The Supporting Information is available free of charge at https://pubs.acs.org/doi/10.1021/jacs.4c05037.

Description of the synthetic procedures and details of general instrumentation; characterization of core and core/shell nanoparticles with HAADF STEM, ^1H and ^{31}P NMR, DLS, powder XRD, PDF, and additional emission and excitation spectra (PDF)

■ AUTHOR INFORMATION

Corresponding Author

Jonathan De Roo − *Department of Chemistry, University of Basel, 4058 Basel, Switzerland;* orcid.org/0000-0002-1264-9312; Email: jonathan.deroo@unibas.ch

Authors

Carlotta Seno − *Department of Chemistry, University of Basel, 4058 Basel, Switzerland;* orcid.org/0000-0002-3565-8086

Nico Reichholf − *Department of Chemistry, University of Basel, 4058 Basel, Switzerland;* orcid.org/0000-0003-4064-3011

Francesco Salutari − *Catalan Institute of Nanoscience and Nanotechnology (ICN2), CSIC and BIST, 08193 Barcelona, Catalonia, Spain*

Maria Chiara Spadaro − *Catalan Institute of Nanoscience and Nanotechnology (ICN2), CSIC and BIST, 08193 Barcelona, Catalonia, Spain; Department of Physics and Astronomy "Ettore Majorana", University of Catania and CNR-IMM, 95123 Catania, Italy;* orcid.org/0000-0002-6540-0377

Yurii P. Ivanov − *Electron Spectroscopy and Nanoscopy, Istituto Italiano di Tecnologia, 16163 Genova, Italy*

Giorgio Divitini − *Electron Spectroscopy and Nanoscopy, Istituto Italiano di Tecnologia, 16163 Genova, Italy;* orcid.org/0000-0003-2775-610X

Alexander Gogos − *Laboratory for Particles-Biology Interactions, Department of Materials Meet Life, Swiss Federal Laboratories for Materials Science and Technology (Empa), 9014 St. Gallen, Switzerland; Nanoparticle Systems Engineering Laboratory, Institute of Process Engineering, Department of Mechanical and Process Engineering, ETH Zurich, 8092 Zurich, Switzerland*

Inge K. Herrmann − *Laboratory for Particles-Biology Interactions, Department of Materials Meet Life, Swiss Federal Laboratories for Materials Science and Technology (Empa), 9014 St. Gallen, Switzerland; Nanoparticle Systems Engineering Laboratory, Institute of Process Engineering, Department of Mechanical and Process Engineering, ETH Zurich, 8092 Zurich, Switzerland*

Jordi Arbiol − *Catalan Institute of Nanoscience and Nanotechnology (ICN2), CSIC and BIST, 08193 Barcelona, Catalonia, Spain; ICREA, 08010 Barcelona, Catalonia, Spain;* orcid.org/0000-0002-0695-1726

Philippe F. Smet − *LumiLab, Department of Solid State Sciences, Ghent University, 9000 Ghent, Belgium;* orcid.org/0000-0003-4789-5799

Complete contact information is available at: https://pubs.acs.org/10.1021/jacs.4c05037

Notes

The authors declare no competing financial interest.

■ ACKNOWLEDGMENTS

C.S. and N.R. thank the SNSF Eccellenza funding scheme (Project 194172) for funding. The authors acknowledge Jikson Pulparayil Mathew for helping with TGA measurements. ICN2 acknowledges funding from Generalitat de Catalunya 2021SGR00457. This study is part of the Advanced Materials Programme and was supported by MCIN with funding from European Union NextGenerationEU (PRTR-C17.I1) and by Generalitat de Catalunya. ICN2 is supported by the Severo Ochoa Program from the Spanish MCIN/AEI (Grant CEX2021-001214-S) and is funded by the CERCA Programme/Generalitat de Catalunya. Part of the present work was performed in the framework of Universitat Autònoma de Barcelona Materials Science Ph.D. program. ICN2 is founding member of e-DREAM.[60] The authors acknowledge the use of instrumentation as well as the technical advice provided by the Joint Electron Microscopy Center at ALBA (JEMCA). ICN2 acknowledges funding from Grant IU16-014206 (METCAM-FIB) funded by the European Union through the European Regional Development Fund (ERDF), with the support of the Ministry of Research and Universities, Generalitat de Catalunya. The authors thank Ralf Kägi and Andreas Voegelin (Eawag, Switzerland) for access to their HF laboratories. We acknowledge DESY (Hamburg, Germany), a member of the Helmholtz Association HGF, for the provision of experimental facilities. Parts of this research were carried out using beamline P21.1 at PETRA III, and the authors thank Ann-Christin Dippel, Jiatu Liu, and Fernando Igoa for assistance in using the beamline for PDF acquisition (Proposal I-20231114 EC). This research also used resources of the Advanced Photon Source, a U.S. Department of Energy (DOE) Office of Science user facility operated for the DOE Office of Science by Argonne National Laboratory under Contract DE-AC02-06CH11357. Part of the experiments were carried out using beamline 11-ID-B (Proposal GUP-81183).

■ REFERENCES

(1) Van den Eynden, D.; Pokratath, R.; De Roo, J. Nonaqueous Chemistry of Group 4 Oxo Clusters and Colloidal Metal Oxide Nanocrystals. *Chem. Rev.* **2022**, *122* (11), 10538−10572.

(2) Tao, P.; Li, Y.; Siegel, R. W.; Schadler, L. S. Transparent dispensible high-refractive index ZrO_2/epoxy nanocomposites for LED encapsulation. *J. Appl. Polym. Sci.* **2013**, *130* (5), 3785−3793.
(3) Liu, C.; Hajagos, T. J.; Chen, D.; Chen, Y.; Kishpaugh, D.; Pei, Q. Efficient one-pot synthesis of colloidal zirconium oxide nanoparticles for high-refractive-index nanocomposites. *ACS Appl. Mater. Interfaces* **2016**, *8* (7), 4795−4802.
(4) De Keukeleere, K.; Cayado, P.; Meledin, A.; Vallès, F.; De Roo, J.; Rijckaert, H.; Pollefeyt, G.; Bruneel, E.; Palau, A.; Coll, M.; et al. Superconducting $YBa_2Cu_3O_{7-\delta}$ nanocomposites using preformed ZrO_2 nanocrystals: growth mechanisms and vortex pinning properties. *Adv. Electron. Mater.* **2016**, *2* (10), 1600161.
(5) Wang, J.; Choudhary, S.; De Roo, J.; De Keukeleere, K.; Van Driessche, I.; Crosby, A. J.; Nonnenmann, S. S. How ligands affect resistive switching in solution-processed HfO_2 nanoparticle assemblies. *ACS Appl. Mater. Interfaces* **2018**, *10* (5), 4824−4830.
(6) Maiti, S.; Ohlerth, T.; Schmidt, N.; Aussen, S.; Waser, R.; Simon, U.; Karthäuser, S. Moisture Effect on the Threshold Switching of TOPO-Stabilized Sub-10 nm HfO_2 Nanocrystals in Nanoscale Devices. *J. Phys. Chem. C* **2022**, *126* (43), 18571−18579.
(7) McGinnity, T. L.; Dominguez, O.; Curtis, T. E.; Nallathamby, P. D.; Hoffman, A. J.; Roeder, R. K. Hafnia (HfO_2) nanoparticles as an X-ray contrast agent and mid-infrared biosensor. *Nanoscale* **2016**, *8* (28), 13627−13637.
(8) Deblock, L.; Descamps, B.; Goemaere, I.; Goossens, E.; Vergauwen, G.; Debacker, J.; Tummers, P.; Remaut, K.; Van Driessche, I.; De Buysser, K.; et al. Dual-Modality Hafnium Oxide Nanocrystals for in Vivo Computed Tomography and Fluorescence Imaging of Sentinel Lymph Nodes. *Chem. Mater.* **2023**, *35* (21), 8883−8896.
(9) Goossens, E.; Deblock, L.; Caboor, L.; Eynden, D. V. D.; Josipovic, I.; Isaacura, P. R.; Maksimova, E.; Van Impe, M.; Bonnin, A.; Segers, P.; et al. From Corrosion Casting to Virtual Dissection: Contrast-Enhanced Vascular Imaging using Hafnium Oxide Nanocrystals. *Small Methods* **2024**, e2301499.
(10) Liu, C.; Hajagos, T. J.; Kishpaugh, D.; Jin, Y.; Hu, W.; Chen, Q.; Pei, Q. Facile Single Precursor Synthesis and Surface Modification of Hafnium Oxide Nanoparticles for Nanocomposite γ Ray Scintillators. *Adv. Funct. Mater.* **2015**, *25* (29), 4607−4616.
(11) Maggiorella, L.; Barouch, G.; Devaux, C.; Pottier, A.; Deutsch, E.; Bourhis, J.; Borghi, E.; Levy, L. Nanoscale radiotherapy with hafnium oxide nanoparticles. *Future Oncol.* **2012**, *8* (9), 1167−1181.
(12) Marill, J.; Anesary, N. M.; Zhang, P.; Vivet, S.; Borghi, E.; Levy, L.; Pottier, A. Hafnium oxide nanoparticles: toward an in vitropredictive biological effect? *Radiat. Oncol.* **2014**, *9* (1), 150.
(13) Bonvalot, S.; Le Pechoux, C.; De Baere, T.; Kantor, G.; Buy, X.; Stoeckle, E.; Terrier, P.; Sargos, P.; Coindre, J. M.; Lassau, N.; et al. First-in-human study testing a new radioenhancer using nanoparticles (NBTXR3) activated by radiation therapy in patients with locally advanced soft tissue sarcomas. *Clin. Cancer Res.* **2017**, *23* (4), 908−917.
(14) Villa, I.; Villa, C.; Monguzzi, A.; Babin, V.; Tervoort, E.; Nikl, M.; Niederberger, M.; Torrente, Y.; Vedda, A.; Lauria, A. Demonstration of cellular imaging by using luminescent and anticytotoxic europium-doped hafnia nanocrystals. *Nanoscale* **2018**, *10* (17), 7933−7940.
(15) Liu, Y.; Zhou, S.; Tu, D.; Chen, Z.; Huang, M.; Zhu, H.; Ma, E.; Chen, X. Amine-functionalized lanthanide-doped zirconia nanoparticles: optical spectroscopy, time-resolved fluorescence resonance energy transfer biodetection, and targeted imaging. *J. Am. Chem. Soc.* **2012**, *134* (36), 15083−15090.
(16) Lauria, A.; Villa, I.; Fasoli, M.; Niederberger, M.; Vedda, A. Multifunctional role of rare earth doping in optical materials: nonaqueous sol-gel synthesis of stabilized cubic HfO_2 luminescent nanoparticles. *ACS Nano* **2013**, *7* (8), 7041−7052.
(17) Ninjbadgar, T.; Garnweitner, G.; Börger, A.; Goldenberg, L. M.; Sakhno, O. V.; Stumpe, J. Synthesis of Luminescent ZrO_2:Eu^{3+} Nanoparticles and Their Holographic Sub-Micrometer Patterning in Polymer Composites. *Adv. Funct. Mater.* **2009**, *19* (11), 1819−1825.
(18) Guichard, X. H.; Lauria, A. Decoupling of the Crystal Structure and Upconversion in HfO_2 Nanocrystals: Emission Chromaticity to Determine the Nanoscale Dopant Distribution. *Chem. Mater.* **2024**, *36* (6), 2623−2633.
(19) Banski, M.; Afzaal, M.; Podhorodecki, A.; Misiewicz, J.; Abdelhady, A.; O'Brien, P. Passivation of lanthanide surface sites in sub-10 nm $NaYF_4$:Eu^{3+} nanocrystals. *J. Nanopart. Res.* **2012**, *14*, 1228.
(20) Wang, F.; Liu, X. Upconversion multicolor fine-tuning: visible to near-infrared emission from lanthanide-doped $NaYF_4$ nanoparticles. *J. Am. Chem. Soc.* **2008**, *130* (17), 5642−5643.
(21) Mai, H.-X.; Zhang, Y.-W.; Si, R.; Yan, Z.-G.; Sun, L.-d.; You, L.-P.; Yan, C.-H. High-Quality Sodium Rare-Earth Fluoride Nanocrystals: Controlled Synthesis and Optical Properties. *J. Am. Chem. Soc.* **2006**, *128* (19), 6426−6436.
(22) Zheng, B.; Fan, J.; Chen, B.; Qin, X.; Wang, J.; Wang, F.; Deng, R.; Liu, X. Rare-Earth Doping in Nanostructured Inorganic Materials. *Chem. Rev.* **2022**, *122* (6), 5519−5603.
(23) Gai, S.; Li, C.; Yang, P.; Lin, J. Recent Progress in Rare Earth Micro/Nanocrystals: Soft Chemical Synthesis, Luminescent Properties, and Biomedical Applications. *Chem. Rev.* **2014**, *114* (4), 2343−2389.
(24) Efros, A. L.; Brus, L. E. Nanocrystal Quantum Dots: From Discovery to Modern Development. *ACS Nano* **2021**, *15* (4), 6192−6210.
(25) Peng, X.; Schlamp, M. C.; Kadavanich, A. V.; Alivisatos, A. P. Epitaxial growth of highly luminescent CdSe/CdS core/shell nanocrystals with photostability and electronic accessibility. *J. Am. Chem. Soc.* **1997**, *119* (30), 7019−7029.
(26) Rabouw, F. T.; Prins, P. T.; Villanueva-Delgado, P.; Castelijns, M.; Geitenbeek, R. G.; Meijerink, A. Quenching pathways in $NaYF_4$:Er^{3+}, Yb^{3+} upconversion nanocrystals. *ACS Nano* **2018**, *12* (5), 4812−4823.
(27) Peng, D.; Ju, Q.; Chen, X.; Ma, R.; Chen, B.; Bai, G.; Hao, J.; Qiao, X.; Fan, X.; Wang, F. Lanthanide-doped energy cascade nanoparticles: full spectrum emission by single wavelength excitation. *Chem. Mater.* **2015**, *27* (8), 3115−3120.
(28) Hanaoka, K.; Kikuchi, K.; Kobayashi, S.; Nagano, T. Time-resolved long-lived luminescence imaging method employing luminescent lanthanide probes with a new microscopy system. *J. Am. Chem. Soc.* **2007**, *129* (44), 13502−13509.
(29) Ramírez-García, G.; Díaz Cervantes, E.; Mounzer, O.; De la Rosa, E.; López Luke, T.; de la Cruz, F. N. A turn-on luminescence method for phosphate determination based on fast green-functionalized ZrO_2:Yb, Er@ZrO_2 core@shell upconversion nanoparticles. *Anal. Chem.* **2019**, *91* (22), 14657−14665.
(30) Zhang, F. *Photon Upconversion Nanomaterials*; Springer, 2015.
(31) Joo, J.; Yu, T.; Kim, Y. W.; Park, H. M.; Wu, F. X.; Zhang, J. Z.; Hyeon, T. Multigrarn scale synthesis and characterization of monodisperse tetragonal zirconia nanocrystals. *J. Am. Chem. Soc.* **2003**, *125* (21), 6553−6557.
(32) Pokratath, R.; Van den Eynden, D.; Cooper, S. R.; Mathiesen, J. K.; Waser, V.; Devereux, M.; Billinge, S. J.; Meuwly, M.; Jensen, K. M.; De Roo, J. Mechanistic Insight into the Precursor Chemistry of ZrO_2 and HfO_2 Nanocrystals; towards Size-Tunable Syntheses. *JACS Au* **2022**, *2* (4), 827−838.
(33) Pokratath, R.; Lermusiaux, L.; Checchia, S.; Mathew, J. P.; Cooper, S. R.; Mathiesen, J. K.; Landaburu, G.; Banerjee, S.; Tao, S.; Reichholf, N.; et al. An Amorphous Phase Precedes Crystallization: Unraveling the Colloidal Synthesis of Zirconium Oxide Nanocrystals. *ACS Nano* **2023**, *17* (9), 8796−8806.
(34) Tang, J.; Fabbri, J.; Robinson, R. D.; Zhu, Y. M.; Herman, I. P.; Steigerwald, M. L.; Brus, L. E. Solid-solution nanopartieles: Use of a nonhydrolytic sol-gel synthesis to prepare HfO_2 and $Hf_xZr_{1-x}O_2$ nanocrystals. *Chem. Mater.* **2004**, *16* (7), 1336−1342.
(35) Waetzig, G. R.; Depner, S. W.; Asayesh-Ardakani, H.; Cultrara, N. D.; Shahbazian-Yassar, R.; Banerjee, S. Stabilizing metastable tetragonal HfO_2 using a non-hydrolytic solution-phase route: ligand exchange as a means of controlling particle size. *Chem. Sci.* **2016**, *7* (8), 4930−4939.

https://doi.org/10.1021/jacs.4c05037
J. Am. Chem. Soc. 2024, 146, 20550−20555

(36) Depner, S. W.; Cultrara, N. D.; Farley, K. E.; Qin, Y.; Banerjee, S. Ferroelastic Domain Organization and Precursor Control of Size in Solution-Grown Hafnium Dioxide Nanorods. *ACS Nano* **2014**, *8* (5), 4678−4688.
(37) Ohlerth, T.; Du, H.; Hammoor, T.; Mayer, J.; Simon, U. Tailoring of Colloidal HfO_2 Nanocrystals with Unique Morphologies and New Self-Assembly Features. *Small Sci.* **2024**, *4* (4), 2300209.
(38) Depner, S. W.; Kort, K. R.; Banerjee, S. Precursor control of crystal structure and stoichiometry in twin metal oxide nanocrystals. *CrystEngComm* **2009**, *11* (5), 841−846.
(39) Robinson, R. D.; Tang, J.; Steigerwald, M. L.; Brus, L. E.; Herman, I. P. Raman scattering in $Hf_xZr_{1-x}O_2$ nanoparticles. *Phys. Rev. B* **2005**, *71* (11), 115408.
(40) Müller, J.; Böscke, T. S.; Bräuhaus, D.; Schröder, U.; Böttger, U.; Sundqvist, J.; Kücher, P.; Mikolajick, T.; Frey, L. Ferroelectric $Zr_{0.5}Hf_{0.5}O_2$ thin films for nonvolatile memory applications. *Appl. Phys. Lett.* **2011**, *99* (11), 112901.
(41) Hwang, J.; Goh, Y.; Jeon, S. Physics, Structures, and Applications of Fluorite Structured Ferroelectric Tunnel Junctions. *Small* **2023**, *20* (9), 2305271.
(42) De Keukeleere, K.; Coucke, S.; De Canck, E.; Van Der Voort, P.; Delpech, F.; Coppel, Y.; Hens, Z.; Van Driessche, I.; Owen, J. S.; De Roo, J. Stabilization of Colloidal Ti, Zr, and Hf Oxide Nanocrystals by Protonated Tri-n-octylphosphine Oxide (TOPO) and Its Decomposition Products. *Chem. Mater.* **2017**, *29* (23), 10233−10242.
(43) McCormack, S. J.; Weber, R. J.; Kriven, W. M. In-situ investigation of $Hf_6Ta_2O_{17}$ anisotropic thermal expansion and topotactic, peritectic transformation. *Acta Mater.* **2018**, *161*, 127−137.
(44) Lutterotti, L.; Scardi, P. Simultaneous structure and size-strain refinement by the Rietveld method. *J. Appl. Crystallogr.* **1990**, *23* (4), 246−252.
(45) Smits, K.; Grigorjeva, L.; Millers, D.; Sarakovskis, A.; Opalinska, A.; Fidelus, J. D.; Lojkowski, W. Europium doped zirconia luminescence. *Opt. Mater.* **2010**, *32* (8), 827−831.
(46) Nashivochnikov, A. A.; Kostyukov, A. I.; Zhuzhgov, A. V.; Rakhmanova, M. I.; Cherepanova, S. V.; Snytnikov, V. N. Shaping the photoluminescence spectrum of ZrO_2:Eu^{3+} phosphor in dependence on the Eu concentration. *Opt. Mater.* **2021**, *121*, 111620.
(47) Nashivochnikov, A. A.; Kostyukov, A. I.; Rakhmanova, M. I.; Cherepanova, S. V.; Snytnikov, V. N. Photoluminescence and structure evolution of laser synthesized ZrO_2:Eu^{3+} nanopowders depending on the dopant concentration. *Ceram. Int.* **2023**, *49* (3), 5049−5057.
(48) Freris, I.; Riello, P.; Enrichi, F.; Cristofori, D.; Benedetti, A. Synthesis and optical properties of sub-micron sized rare earth-doped zirconia particles. *Opt. Mater.* **2011**, *33* (11), 1745−1752.
(49) Speghini, A.; Bettinelli, M.; Riello, P.; Bucella, S.; Benedetti, A. Preparation, structural characterization, and luminescence properties of Eu^{3+}-doped nanocrystalline ZrO_2. *J. Mater. Res.* **2005**, *20* (10), 2780−2791.
(50) Binnemans, K. Interpretation of europium(III) spectra. *Coord. Chem. Rev.* **2015**, *295*, 1−45.
(51) Opitz, L.; Hübner, R.; Shams Aldin Azzam, S.; Gilson, S. E.; Finkeldei, S. C.; Huittinen, N. Investigations towards incorporation of Eu^{3+} and Cm^{3+} during ZrO_2 crystallization in aqueous solution. *Sci. Rep.* **2023**, *13* (1), 12276.
(52) Ghosh, P.; Patra, A. Role of surface coating in ZrO_2/Eu^{3+} nanocrystals. *Langmuir* **2006**, *22* (14), 6321−6327.
(53) Emeline, A.; Kataeva, G. V.; Litke, A. S.; Rudakova, A. V.; Ryabchuk, V. K.; Serpone, N. Spectroscopic and photoluminescence studies of a wide band gap insulating material: powdered and colloidal ZrO_2 sols. *Langmuir* **1998**, *14* (18), 5011−5022.
(54) Carvalho, J. M.; Rodrigues, L. C.; Hölsä, J.; Lastusaari, M.; Nunes, L. A.; Felinto, M. C.; Malta, O. L.; Brito, H. F. Influence of titanium and lutetium on the persistent luminescence of ZrO_2. *Opt. Mater. Express* **2012**, *2* (3), 331−340.
(55) Prakashbabu, D.; Hari Krishna, R.; Nagabhushana, B. M.; Nagabhushana, H.; Shivakumara, C.; Chakradar, R. P. S.; Ramalingam, H. B.; Sharma, S. C.; Chandramohan, R. Low temperature synthesis of pure cubic ZrO_2 nanopowder: Structural and luminescence studies. *Spectrochim. Acta, Part A* **2014**, *122*, 216−222.
(56) Li, L.; Qu, X.; Pan, G.-H.; Jeong, J. H. Novel Photoluminescence and Optical Thermometry of Solvothermally Derived Tetragonal ZrO_2:Ti^{4+}, Eu^{3+} Nanocrystals. *Chemosensors* **2024**, *12* (4), 62.
(57) Ponnilavan, V.; Kannan, S. Structural, optical tuning, and mechanical behavior of zirconia toughened alumina through europium substitutions. *J. Biomed. Mater. Res., Part B* **2019**, *107* (4), 1170−1179.
(58) Villabona-Leal, E.; Diaz-Torres, L.; Desirena, H.; Rodríguez-López, J.; Pérez, E.; Meza, O. Luminescence and energy transfer properties of Eu^{3+} and Gd^{3+} in ZrO_2. *J. Lumin.* **2014**, *146*, 398−403.
(59) King, A.; Singh, R.; Nayak, B. B. Phase and photoluminescence analysis of dual-color emissive Eu^{3+}-doped ZrO_2 nanoparticles for advanced security features in anti-counterfeiting. *Colloids Surf., A* **2021**, *631*, 127715.
(60) Ciancio, R.; Dunin-Borkowski, R. E.; Snoeck, E.; Kociak, M.; Holmestad, R.; Verbeeck, J.; Kirkland, A. I.; Kothleitner, G.; Arbiol, J. e-DREAM: the European Distributed Research Infrastructure for Advanced Electron Microscopy. *Microsc. Microanal.* **2022**, *28* (S1), 2900−2902.

https://doi.org/10.1021/jacs.4c05037
J. Am. Chem. Soc. 2024, 146, 20550−20555